



A Quasi-LPV Approach for Gain Scheduling Cascaded NDI-based Controllers for Hypersonic Glide Vehicles

Johannes Autenrieb*, Nicolas Fezans†

German Aerospace Center (DLR), Institute of Flight Systems, 38108, Braunschweig, Germany

Patrick Gruhn‡

German Aerospace Center (DLR), Institute of Aerodynamics and Flow Technology, 51147, Cologne, Germany

Hypersonic glide vehicles (HGVs) have emerged as crucial assets with applications in both civil and military sectors, prompting significant research and development efforts. Ensuring the stability and precision of these vehicles, especially in the face of complex and uncertain physical effects, necessitates well-designed autopilots and robust control systems. Among the control methodologies explored, nonlinear dynamic inversion (NDI) stands out as a promising approach, offering the ability to handle highly nonlinear systems effectively. However, challenges such as sensitivity to model uncertainties and closed-loop instabilities pose significant hurdles. Addressing these challenges requires careful consideration of closed-loop dynamics, either through robust control approaches or tailored pole locations. This paper proposes a systematic methodology for determining suitable gains for cascaded nonlinear controllers, leveraging the similarities between NDI and quasi-linear parameter-varying (quasi-LPV) systems. By transforming nested nonlinear dynamics into a quasi-LPV framework, the proposed approach enables the utilization of linear control tools, providing stability and performance across the entire flight envelope. The contributions of the paper include discussions on the transformation of nonlinear dynamics, validations of assumptions, insights into potential applications of quasi-LPV control, and simulation results demonstrating the effectiveness of the proposed methodology.

I. Introduction

In recent years, hypersonic glide vehicles (HGVs) have increasingly become the subject of research and development efforts from both academia and industry [1]. This emerging class of vehicles has potential applications in both civil and military sectors [2]. The German Aerospace Center (DLR) is investigating autonomous hypersonic flight systems' physical limitations and performance across various mission scenarios. Robustly designed autopilots are essential for autonomous flight vehicles, as they stabilize the vehicle and ensure precise tracking of either online or offline computed trajectories to reach desired destinations. Control systems must manage complex and uncertain physical effects across expansive flight envelopes for hypersonic applications.

Nonlinear dynamic inversion (NDI) is a control approach well-suited for handling the highly nonlinear characteristics of hypersonic glide vehicles throughout the envelope. The primary benefit of NDI is the simplification of the input-output dynamics of a nonlinear, input-affine system by using state feedback and coordinate transformation rather than traditional Jacobian Linearization [3]. This reduction transforms the dynamics of the controlled variables to simple integrator dynamics, enabling control through a single linear controller [4]. Successful applications of cascaded NDI feedback controllers have been demonstrated, such as in [5] for autonomous attitude control of hypersonic re-entry vehicles and in [6] for control augmentation in supermaneuverable aircraft. Both cases employ time-scale separation to address the nested attitude dynamics [7].

NDI, despite its benefits, presents notable challenges. It is sensitive to inaccuracies in the underlying model due to its model-based online linearization, which can lead to inversion errors and closed-loop instabilities [8]. This sensitivity underscores the need for robustness in control design [9–11]. While NDI theoretically enables uniform closed-loop dynamics across an entire flight envelope, this concept often conflicts with robustness requirements, particularly in systems with broad flight envelopes like hypersonic vehicles. Significant variations in open-loop dynamics can

*Research Scientist, Department of Flight Dynamics and Simulation, email:johannes.autenrieb@dlr.de

†Scientific Advisor, Department of Flight Dynamics and Simulation, email:nicolas.fezans@dlr.de

‡Head of Missile Technologies Group, Department of Supersonic and Hypersonic Technologies, email:patrick.gruhn@dlr.de

overburden actuators when closed-loop dynamics designed for specific operating points are enforced across the envelope. Furthermore, cascaded NDI controllers, often tuned manually and independently, fail to account for interactions between loops, resulting in overlooked gain and phase margin requirements. These issues, compounded by practical constraints like measurement inaccuracies and actuator limitations, often degrade real-world performance. Though NDI theoretically removes the need for gain scheduling, incorporating it can improve robustness by addressing open-loop dynamic variations across extensive flight envelopes.

Motivated by the identified challenges in robustness and tuning of NDI-based cascaded control systems, this paper leverages the connections between NDI- and LPV-based methodologies to establish a systematic controller design workflow for HGVs during the midcourse phase. Fig. 1 provides an overview of the mission phases of an HGV and gives context to the midcourse phase. The mission begins with the launch phase, followed by the separation and reentry phase, where the HGV detaches from the launch vehicle at approximately 100 km altitude. The subsequent midcourse phase occupies most of the mission time and involves atmospheric gliding at high speeds with a trajectory optimized for maximum lift-to-drag ratio. The mission ends in the terminal phase, where the vehicle executes precise maneuvers to approach and impact its target. To clarify the operational environment, it is essential to distinguish between exoatmospheric and endoatmospheric flight conditions. During exoatmospheric flight, which occurs at altitudes where aerodynamic control surfaces are no longer effective due to insufficient atmospheric density, small integrated propulsors generate the necessary moments to control the vehicle's attitude. In contrast, during endoatmospheric flight, within atmospheric conditions, four integrated flaps are employed as control effectors, cf. Fig. 4.

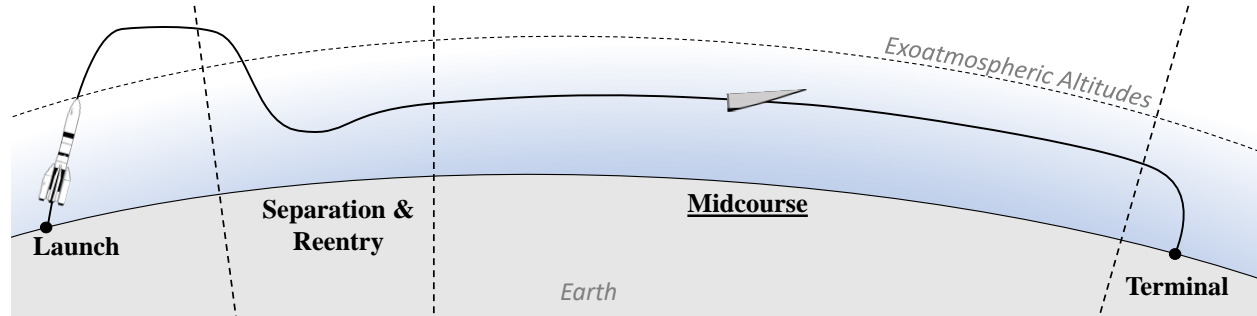


Figure 1 Mission phases of HGV.

The here proposed unified framework addresses the difficulties of managing operations across the large flight envelope of HGVs, particularly during the midcourse phase. The proposed method provides robustness against model inaccuracies, parametric uncertainties, and actuator constraints. By integrating the method into the control design workflow, this approach offers a structured solution for tuning cascaded NDI controllers throughout the flight envelope, ensuring optimal performance under varying conditions.

The main contributions of this paper are threefold. First, a quasi-LPV framework is developed, tailored explicitly for the nonlinear dynamics of HGVs during the midcourse. This enables the application of established linear control techniques for the tuning of cascaded NDI controllers at different operating points within the flight envelope. Second, the assumptions underlying the proposed approach are validated by comparing the derived quasi-LPV model with the full nonlinear system dynamics, ensuring consistency and accuracy across the flight envelope. Third, the controller's performance is evaluated through a simulation-based analysis using a high-fidelity model of a hypersonic vehicle.

The paper is organized as follows: Section II provides an overview of the nonlinear dynamics model for the hypersonic glide vehicle. Section III introduces the fundamental design principles of the cascaded controller-based NDI. Section IV presents the quasi-LPV system approach used to convert the vehicle's nonlinear dynamics into a quasi-LPV state-space model. Additionally, Section V details the application of Eigenstructure assignment, offering an efficient and straightforward control design workflow. This design framework aims to produce a nonlinear control architecture with closed-loop poles at targeted locations, ensuring stability and robust performance across the flight envelope. Finally, Section VI discusses a simulation-based evaluation of the proposed control system's performance.

II. Nonlinear Flight Dynamics

The nonlinear simulation model of the Generic Hypersonic Glide Vehicle 2 (GHGV-2), which is the application example of the methods presented in this paper, was developed with colleagues from the DLR Institute of Aerodynamics

and Flow Technology. The simulation is implemented in MATLAB/Simulink and focuses on the flight control system design of the regarded hypersonic flight vehicle. The relevant properties for this work are provided in the following, but interested readers are referred to [12] for further details. In the current state, the aerodynamic database considers static and dynamic aerodynamic effects modeled as static and dynamic derivative coefficients. The aerodynamic coefficients were calculated by computational fluid dynamics using the DLR TAU code [13, 14]. Around 800 inviscid calculations were performed for a broad set of Mach numbers, angles of attack, angles of sideslip, and control surface deflection angles. The environmental conditions for each Mach number were based on the atmospheric conditions at a specific altitude taken from a pre-determined trajectory. To consider viscous effects, fully viscous Reynolds-averaged Navier-Stokes simulations were performed for selected trajectory points.

The modeled nonlinear flight dynamics of the GHGV-2 are based on classical Newtonian mechanics, in which the vehicle is assumed as a rigid body. The notation convention used for the flight mechanical quantities follows the standard notations for flight mechanical quantities from [15, 16]. Fig. 2 displays the components of the total external forces X , Y , Z and the total external moments L , M , N expressed in the body-fixed frame of the vehicle. For the investigated case, only the aerodynamic and gravitational forces and moments are considered relevant during the reentry and glide phases since hypersonic glide vehicles are commonly unpropelled during those mission stages. Centrifugal and Coriolis forces, that originate from motions within a moving reference system (consideration of Earth's rotation), are additionally computed and taken into account as external forces in the body-fixed frame. Atmospheric effects were modeled using the International Standard Atmosphere (ISA) [17]: Eq. (1) and Eq. (2) present the generalized equations of motion for

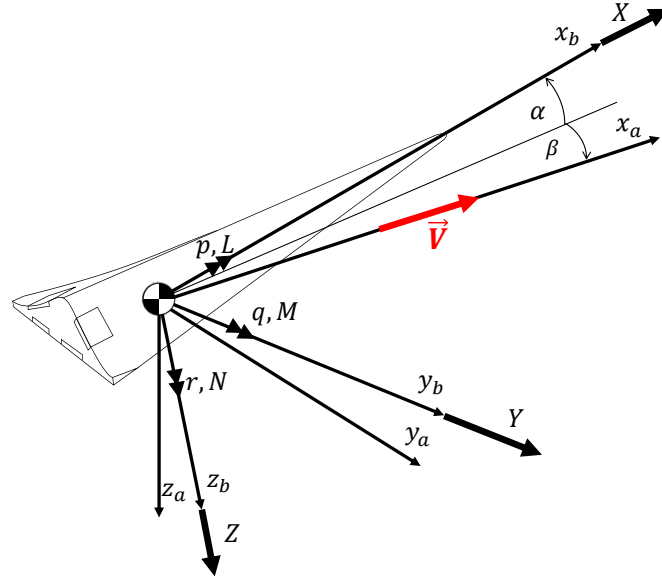


Figure 2 Sketch of external forces and moments attacking on the GHGV-2 concept [12].

translation and rotation of a flight vehicle as:

$$\vec{R} = \begin{bmatrix} X \\ Y \\ Z \end{bmatrix} = m \begin{bmatrix} \dot{u}_K \\ \dot{v}_K \\ \dot{w}_K \end{bmatrix} + m \begin{bmatrix} p_K \\ q_K \\ r_K \end{bmatrix} \times \begin{bmatrix} u_K \\ v_K \\ w_K \end{bmatrix}, \quad (1)$$

$$\vec{Q} = \begin{bmatrix} L \\ M \\ N \end{bmatrix} = I \begin{bmatrix} \dot{p}_K \\ \dot{q}_K \\ \dot{r}_K \end{bmatrix} + \begin{bmatrix} p_K \\ q_K \\ r_K \end{bmatrix} \times I \begin{bmatrix} p_K \\ q_K \\ r_K \end{bmatrix}. \quad (2)$$

The used variables are defined as the mass m , the Moment of inertia I , the body-fixed rotational rates in the inertial axes $(p_K, q_K, r_K)^T$ and the body-fixed translational velocity in the inertial axes $(u_K, v_K, w_K)^T$, denoted by the index K . An important kinematic relationship that connects the time derivatives of the flight-path bank angle μ_K , the inertial angle of attack α_K and the inertial sideslip angle β_K to the body-fixed rotational rates and the corresponding time derivatives of the flight path angle γ and track angle χ , can be stated as:

$$\begin{aligned} \begin{bmatrix} \dot{\mu}_K \\ \dot{\alpha}_K \\ \dot{\beta}_K \end{bmatrix} &= T_1 \begin{bmatrix} p_K \\ q_K \\ r_K \end{bmatrix} + T_2 \begin{bmatrix} \dot{\gamma} \\ \dot{\chi} \end{bmatrix} \\ &= \begin{bmatrix} \frac{\cos \alpha_K}{\cos \beta_K} & 0 & \frac{\sin \alpha_K}{\cos \beta_K} \\ -\cos \alpha_K \tan \beta_K & 1 & -\sin \alpha_K \tan \beta_K \\ \sin \alpha_K & 0 & -\cos \alpha_K \end{bmatrix} \begin{bmatrix} p_K \\ q_K \\ r_K \end{bmatrix} + \begin{bmatrix} \cos \mu_K \tan \beta_K & \sin \gamma + \sin \mu_K \tan \beta_K \cos \gamma \\ -\frac{\cos \mu_K}{\cos \beta_K} & -\frac{\sin \mu_K \cos \gamma}{\cos \beta_K} \\ -\sin \mu_K & \cos \mu_K \cos \gamma \end{bmatrix} \begin{bmatrix} \dot{\gamma} \\ \dot{\chi} \end{bmatrix}. \end{aligned} \quad (3)$$

Eq. (3) constitutes a kinematic relationship between various reference frames. In this equation, the rotational rates p_K , q_K , and r_K are obtained from the integration of the moment equation of Eq. (2). Eq. (3) express a general kinematic relationship that also stays valid for cases in which the described aerial vehicle operates in windy conditions. However, to simplify the notation in this paper, wind effects are neglected. This assumption is commonly applied to hypersonic vehicles because their speeds are significantly higher than typical wind velocities [18]. Consequently, the resulting errors in the angle of attack and sideslip angle are negligible, allowing the simplification without a loss of generality. In that case, the inertial axes correspond with the aerodynamic axes. This simplifies the notation during the rest of the paper, describing the body-rate vector in the inertial axes, denoted by the index K , without the corresponding index.

III. Cascaded Nonlinear Controller Design

Fig. 3 shows the integrated NDI-based feedback controller, with distinct linear controllers for the attitude and body-rate control. The cascaded feedback control approach is based on the idea of time-scale separated nonlinear dynamic inversion systems [7]. The developed NDI feedback control system is similar to the feedback control architectures proposed in [6] and [5] but is adapted to match the technical realization of the controlled GHGV-2 [19]. The implementation of the feedback control system is introduced and discussed below.

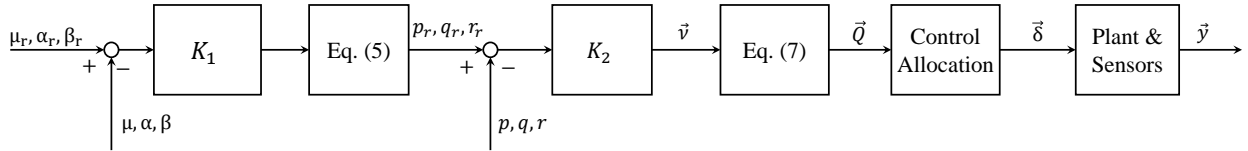


Figure 3 Cascaded inversion-based nonlinear flight control architecture.

The linear outer-loop controller computes the required time derivatives of the aerodynamic angles $(\dot{\mu}_r, \dot{\alpha}_r, \dot{\beta}_r)^T$ needed for reference tracking based error vector $(e_\mu, e_\alpha, e_\beta)^T$, which in turn is computed based on the state measurements $(\mu, \alpha, \beta)^T$ and the obtained reference signals $(\mu_r, \alpha_r, \beta_r)^T$:

$$\begin{bmatrix} \dot{\mu}_r \\ \dot{\alpha}_r \\ \dot{\beta}_r \end{bmatrix} = K_1 \begin{bmatrix} e_\mu \\ e_\alpha \\ e_\beta \end{bmatrix} = K_1 \left(\begin{bmatrix} \mu_r \\ \alpha_r \\ \beta_r \end{bmatrix} - \begin{bmatrix} \mu \\ \alpha \\ \beta \end{bmatrix} \right), \quad (4)$$

with K_1 being a gain matrix. Given the kinematic relationship shown in Eq. (4), the commanded signal vector $(\dot{\mu}_r, \dot{\alpha}_r, \dot{\beta}_r)^T$ can be transformed into a commanded body-rate signal $(p_r, q_r, r_r)^T$ for the inner-loop controller with the following inversion law:

$$\vec{\omega}_r = \begin{bmatrix} p_r \\ q_r \\ r_r \end{bmatrix} = T_1^{-1} \left(\begin{bmatrix} \dot{\mu}_r \\ \dot{\alpha}_r \\ \dot{\beta}_r \end{bmatrix} - T_2 \begin{bmatrix} \dot{\gamma} \\ \dot{\chi} \end{bmatrix} \right), \quad (5)$$

with the T_1 and T_2 matrices defined in Eq. (3). The linear inner-loop controller calculates the overall virtual control command vector \vec{v} (angular acceleration commands) based on the tracking error vector $(e_p, e_q, e_r)^T$, which is computed

using the body-rate state measurements $(p, q, r)^T$ and the obtained reference signals from the prior angular kinematics inversion step:

$$\vec{v} = K_2 \begin{bmatrix} e_p \\ e_q \\ e_r \end{bmatrix} = K_2 \left(\begin{bmatrix} p_r \\ q_r \\ r_r \end{bmatrix} - \begin{bmatrix} p \\ q \\ r \end{bmatrix} \right), \quad (6)$$

with K_2 being a gain matrix. The required moment vector is computed via:

$$\vec{Q} = \begin{bmatrix} L_c \\ M_c \\ N_c \end{bmatrix} = I \begin{bmatrix} \dot{p}_c \\ \dot{q}_c \\ \dot{r}_c \end{bmatrix} + \begin{bmatrix} p \\ q \\ r \end{bmatrix} \times I \begin{bmatrix} p \\ q \\ r \end{bmatrix}. \quad (7)$$

During the midcourse operation at atmospheric altitudes, the GHGV-2 commands a redundant set of control surfaces (four integrated fins) used for the vehicle's attitude control. Fig. 4 shows the available control effectors with the connected deflections of the upper left fin δ_1 , upper right fin δ_2 , lower left fin δ_3 and lower right fin δ_4 . Due to the

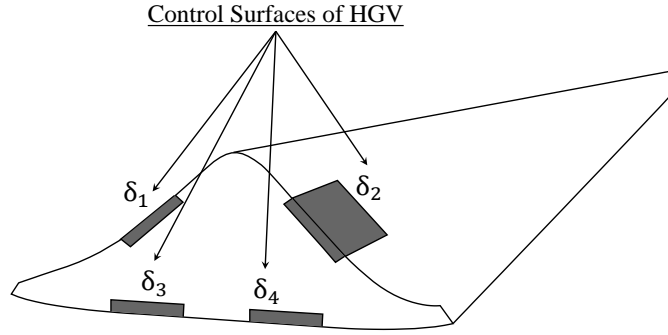


Figure 4 Rear view on GHGV-2 and available control effectors during endoatmospheric operations.

over-actuation of the system, a control allocation system is needed to translate the abstract moment vector \vec{Q} into a control input vector $\vec{\delta}$. To do so, the following constrained min-norm control allocation problem is solved [20–22]:

$$\begin{aligned} & \arg \min_{\vec{\delta} \in \mathbb{R}^m} \|\vec{\delta}\|_2 \\ & \text{subject to } \vec{Q} = B \vec{\delta}, \\ & \vec{\delta}_{min} \leq \vec{\delta} \leq \vec{\delta}_{max}, \end{aligned} \quad (8)$$

where $\vec{\delta}_{min}$, $\vec{\delta}_{max}$, $\vec{\delta}_{min}$ and $\vec{\delta}_{max}$ are maximum and minimum magnitude and rate limits of the redundant set of actuators, m the number of control inputs and B being the control effectiveness matrix defined as the following Jacobian matrix:

$$B = \begin{bmatrix} \frac{\partial L}{\partial \delta_1} & \frac{\partial L}{\partial \delta_2} & \frac{\partial L}{\partial \delta_3} & \frac{\partial L}{\partial \delta_4} \\ \frac{\partial M}{\partial \delta_1} & \frac{\partial M}{\partial \delta_2} & \frac{\partial M}{\partial \delta_3} & \frac{\partial M}{\partial \delta_4} \\ \frac{\partial N}{\partial \delta_1} & \frac{\partial N}{\partial \delta_2} & \frac{\partial N}{\partial \delta_3} & \frac{\partial N}{\partial \delta_4} \end{bmatrix}. \quad (9)$$

Since the l_2 norm is minimized, the optimization problem can be formulated as a quadratic programming control allocation problem, cf. [20, 21].

Remark 1 In the following sections, different concepts and notations for control inputs are used. Due to the over-actuation of the considered hypersonic system, the integrated nonlinear controller described earlier does not directly generate a usable control input for the system. Instead, it produces a virtual control command \vec{v} , which is fed into a control allocation system to compute the control deflections $\vec{\delta}$. These deflections act as the actual control input to the system. In subsequent sections, a generalized view of the control system is presented. To remain consistent with the available literature, the generalized control input vector is denoted as \vec{u} . This vector corresponds with the virtual control command \vec{v} generated by the nonlinear controller in the later introduced methodology.

IV. Quasi-LPV Flight Dynamics Model

As discussed in the previous section, the considered dynamics can be interpreted as nested dynamics, in which the changes in the moment vector lead to body-rate changes and consequently to changes in the vehicle attitude. The following section introduces the general concepts of LPV-based control methodologies and their application to control problems like the one at hand. Subsequently, the steps required to transform the previously introduced nonlinear dynamics of the hypersonic glide vehicle into a parameter-dependent quasi-linear system are outlined. This transformation is later shown to enable a more systematic derivation of the gains for the cascaded linear controllers utilized within an NDI-based control scheme, as detailed in Sect. III, and to facilitate their tuning across different operating points within the flight envelope.

A. Generalities and Grid-Based Quasi-LPV Structure

We consider the following general nonlinear parameter-dependent system:

$$\dot{\vec{x}} = f(\vec{x}(t), \vec{u}(t), \vec{\sigma}(t)), \quad (10)$$

$$\vec{y} = h(\vec{x}(t), \vec{u}(t), \vec{\sigma}(t)), \quad (11)$$

where $\vec{x}(t) \in \mathbb{R}^n$ is the system state, $\vec{u}(t) \in \mathbb{R}^m$ is the control input, $\vec{y}(t) \in \mathbb{R}^p$ is the output vector and $\vec{\sigma}(t) \in \mathbb{R}^q$ represents the operating point parameter vector. In classical flight control approaches, the airframe is trimmed at an operating point, defined by the parameter vector $\vec{\sigma}_0$, by finding the equilibrium controls \vec{u}_0 such that the system state derivative $\dot{\vec{x}} = \frac{\partial \vec{x}}{\partial t}$ goes to zero. As long the system operates in proximity to the considered equilibrium $\vec{\sigma}_0$ while maintaining the trim state \vec{x}_0 and trim control input \vec{u}_0 with additional small $\delta\vec{x}$ and $\delta\vec{u}$ perturbation terms, the dynamics can be approximated using the state-space representation of the form:

$$\delta\dot{\vec{x}} = A(\vec{\sigma}_0) \delta\vec{x}(t) + B(\vec{\sigma}_0) \delta\vec{u}(t), \quad (12)$$

$$\delta\vec{y} = C(\vec{\sigma}_0) \delta\vec{x}(t) + D(\vec{\sigma}_0) \delta\vec{u}(t), \quad (13)$$

where $\delta\vec{x} = \vec{x} - \vec{x}_0$ is the state perturbation vector, $\delta\vec{u} = \vec{u} - \vec{u}_0$ is the input perturbation vector, and $\delta\vec{y} = \vec{y} - \vec{y}_0$ is the output perturbation vector. The matrices $A(\vec{\sigma}_0)$, $B(\vec{\sigma}_0)$, $C(\vec{\sigma}_0)$, and $D(\vec{\sigma}_0)$ represent the Jacobian linearization of the nonlinear system around the trim point $\vec{\sigma}_0$ from Eq. (10) and Eq. (11) in the form of

$$A := \left. \frac{\partial f}{\partial \vec{x}} \right|_{\substack{\vec{x}=\vec{x}_0 \\ \vec{y}=\vec{y}_0 \\ \vec{\sigma}=\vec{\sigma}_0}} \in \mathbb{R}^{n \times n}, \quad B := \left. \frac{\partial f}{\partial \vec{u}} \right|_{\substack{\vec{x}=\vec{x}_0 \\ \vec{y}=\vec{y}_0 \\ \vec{\sigma}=\vec{\sigma}_0}} \in \mathbb{R}^{n \times m},$$

$$C := \left. \frac{\partial h}{\partial \vec{x}} \right|_{\substack{\vec{x}=\vec{x}_0 \\ \vec{y}=\vec{y}_0 \\ \vec{\sigma}=\vec{\sigma}_0}} \in \mathbb{R}^{p \times n}, \quad D := \left. \frac{\partial h}{\partial \vec{u}} \right|_{\substack{\vec{x}=\vec{x}_0 \\ \vec{y}=\vec{y}_0 \\ \vec{\sigma}=\vec{\sigma}_0}} \in \mathbb{R}^{p \times m}.$$

Remark 2 In the case of HGVs, the notion of trim differs slightly from that of conventional subsonic or transonic vehicles. Due to its glide-oriented operation and the absence of integrated propulsion systems after re-entry, the vehicle, unlike standard aircraft, does not typically maintain a steady "1g" horizontal flight. Instead, it continually changes speed and altitude during its mission. For a conventional aircraft, trim is obtained by setting the vector $(\dot{u}, \dot{v}, \dot{w}, \dot{p}, \dot{q}, \dot{r}) = \mathbf{0}_{1 \times 6}$ [23]. However, for the HGV considered here, the trim condition is defined as $(\dot{p}, \dot{q}, \dot{r}, p, r, \dot{\alpha}) = \mathbf{0}_{1 \times 6}$. This condition implies the following: the vehicle is neither rolling nor yawing, and it is not subject to rotational accelerations $(\dot{p}, \dot{q}, \dot{r}, p, r = 0)$. Additionally, $\dot{\alpha} = 0$ means that the angle of attack α and the pitching rate q are determined such that the lift force generated at the given angle of attack balances the current flight path angular rate $\dot{\gamma}$. Furthermore, the control surface deflections required to maintain a constant angle of attack are also specified under this condition.

The obtained state-space system can be used to analyze the dynamics and to derive controllers for a region of attraction around $\vec{\sigma}_0$. Since aerospace systems usually operate over a broad set of equilibria, referred to as flight envelope, an equilibrium manifold must be obtained. Hence, the airframe is trimmed over the whole flight envelope. The different controllers are then connected via interpolation and parameterized as a function of $\vec{\sigma}(t)$; the method is referred to as gain scheduling. NDI-based approaches, as presented in Sect. III, can substitute the gain scheduling by continuously transforming the nonlinear dynamics into the linear domain using known plant dynamics [24].

The same goes for LPV methodologies, which use a state transformation to remove all the nonlinearities present in the model that do not depend on the scheduling variables [25, 26]. The obtained point-wise linear model $S(\vec{\rho})$ can be called an LPV system when its state-space matrices, which are parameterized by the parameter vector $\vec{\rho}$, exclusively depend on the trimming vector, meaning $\vec{\rho} = \vec{\sigma}$. Fig. 5 illustrates the described idea behind the concept of LPV systems. When $\vec{\rho}$ additionally depends on some system states \vec{x} , e.g. $\vec{\rho} = [x_1, x_3, \dots, \sigma]$, the derived model is called quasi-LPV

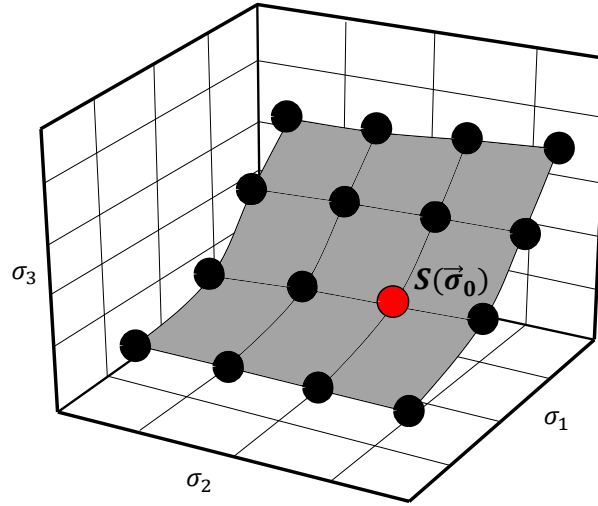


Figure 5 Example for an equilibrium manifold with the parametrization vector $\vec{\sigma} = [\sigma_1, \sigma_2, \sigma_3]^T$ and with an LPV model $S(\vec{\sigma})$ at the trim point $\vec{\sigma}_0$.

[27]. The quasi-LPV model of a general nonlinear system presented in Eq. (10) and Eq. (11) is expressed in a generic form as:

$$S(\vec{\rho}) : \begin{bmatrix} \delta\vec{x}(t) \\ \delta\vec{y}(t) \end{bmatrix} = \begin{bmatrix} A(\vec{\rho}) & B(\vec{\rho}) \\ C(\vec{\rho}) & D(\vec{\rho}) \end{bmatrix} \begin{bmatrix} \delta\vec{x}(t) \\ \delta\vec{u}(t) \end{bmatrix}, \quad (14)$$

Several methods have been proposed to obtain the quasi-LPV model from nonlinear systems as defined in Eq. (10) and Eq. (11), such as state transformation and function substitution [25, 28, 29]. A grid-based quasi-LPV model for modeling the considered dynamics is used in this work. Within the approach, Jacobian linearized dynamics are obtained for a sufficiently large number of operating points over the equilibrium manifold and then connected via interpolation utilizing the parameter vector $\vec{\rho}$ [30]. Fig. 5 illustrates the described idea behind the concept of such grid-based LPV system representations in the case of a three-dimensional dependency.

The flight envelope of a hypersonic glide vehicle system is typically defined by borders which are function of the Mach number Ma and altitude H . Accordingly, an operating point for the system can be defined by the vector of flight point parameters:

$$\vec{\sigma} = \begin{bmatrix} Ma & H \end{bmatrix}^T. \quad (15)$$

If only $\vec{\sigma}$ were considered, the system could indeed be represented as a classical linear parameter-varying (LPV) system. However, the system under consideration is nonlinear with respect to the aerodynamic angles of attack α and sideslip β . As such, relying solely on $\vec{\sigma}$ to capture the system dynamics is insufficient. To address these nonlinearities, α and β are included in the parameter vector:

$$\vec{\rho} = \begin{bmatrix} \alpha & \beta & \vec{\sigma}^T \end{bmatrix}^T = \begin{bmatrix} \alpha & \beta & Ma & H \end{bmatrix}^T. \quad (16)$$

This inclusion transforms the system into a quasi-LPV representation. Since the nonlinearities in α and β are accounted for in the quasi-LPV model, the system dynamics are represented more accurately across the flight envelope.

For the case of midcourse attitude control of HGVs considered in this paper, as suggested in Sect. III, the state vector \vec{x}_δ and the input vector \vec{u}_δ of the considered hypersonic glide vehicle rotational dynamics are defined as follows:

$$\delta\vec{x} = \begin{bmatrix} \delta\vec{x}_1 & \delta\vec{x}_2 \end{bmatrix}^T = \begin{bmatrix} \delta\mu & \delta\alpha & \delta\beta & \delta p & \delta q & \delta r \end{bmatrix}^T \quad (17)$$

$$\delta\vec{u} = \begin{bmatrix} \delta\dot{p} & \delta\dot{q} & \delta\dot{r} \end{bmatrix}^T. \quad (18)$$

with

$$[\delta\mu \ \delta\alpha \ \delta\beta \ \delta p \ \delta q \ \delta r]^T = [\mu \ \alpha \ \beta \ p \ q \ r]^T - [\mu_0 \ \alpha_0 \ \beta_0 \ p_0 \ q_0 \ r_0]^T.$$

$$[\delta\dot{p} \ \delta\dot{q} \ \delta\dot{r}]^T = [\dot{p} \ \dot{q} \ \dot{r}]^T - [\dot{p}_0 \ \dot{q}_0 \ \dot{r}_0]^T.$$

It needs to be noted that for simplicity, in this paper, perfect measurement of the regarded state vector \vec{x} is assumed, which suggests $\vec{y} = \vec{x}$ and leads to $C(\vec{\rho}) = I_{p \times n}$. Further, it is assumed that the control inputs do not have any direct influences on the output vector \vec{y} and hence $D(\vec{\rho}) = 0_{p \times m}$. Both assumptions are commonly used in flight control and hence are not too limiting, as, for example, shown in [31]. However, if the state vector cannot be fully measured, the approach must be extended to an output feedback controller.

B. Derivation of a Grid-Based Quasi-LPV Model for HGVs during the Midcourse Phase

The relationship from Eq. (3) relates the attitude angle time-derivatives ($\dot{\mu}$, $\dot{\alpha}$, $\dot{\beta}$) with the body rates (p , q , r) and flight path angle γ and track angle time-derivatives $\dot{\chi}$. For the application to the aerodynamic attitude control of the hypersonic glider during the midcourse phase, this relationship can be simplified. We first consider the nonlinear dynamics of $\dot{\gamma}$ and $\dot{\chi}$, defined as:

$$\dot{\gamma} = \frac{1}{mV} \underbrace{[L \cos(\mu) - W \cos(\gamma) - Y \sin(\mu) \cos(\beta)]}_{f_\gamma}, \quad (19)$$

where L is the aerodynamic lift force, $W = mg$ is the gravitational force and Y is the aerodynamic side force for $\dot{\gamma}$. For $\dot{\chi}$ Eq. (3) reads:

$$\dot{\chi} = \frac{1}{mV \cos(\gamma)} \underbrace{[L \sin(\mu) + Y \cos(\mu) \cos(\beta)]}_{f_\chi}. \quad (20)$$

To empathize the rationals behind the approach of simplification, a case is constructed in which the vehicle is considered at a parameterized operating point $\vec{\rho}_0 = (\alpha_0, \beta_0, \text{Ma}_0, H_0)$. The dynamics for $\dot{\gamma}$ and $\dot{\chi}$ around the considered point of the equilibrium manifold can be described as perturbation-based dynamics, defined as:

$$\delta\dot{\gamma} = \frac{1}{mV_0} \left[\frac{\partial f_\gamma}{\partial \vec{x}_0}(\vec{x}_0, \vec{u}_0) \delta\vec{x} + \frac{\partial f_\gamma}{\partial \vec{u}_0}(\vec{x}_0, \vec{u}_0) \delta\vec{u} \right], \quad (21)$$

and

$$\delta\dot{\chi} = \frac{1}{mV_0} \left[\frac{\partial f_\chi}{\partial \vec{x}_0}(\vec{x}_0, \vec{u}_0) \delta\vec{x} + \frac{\partial f_\chi}{\partial \vec{u}_0}(\vec{x}_0, \vec{u}_0) \delta\vec{u} \right], \quad (22)$$

where the variable V_0 represents the, in comparison to the regarded attitude dynamics, slow varying travel speed at the considered operating point, which can be expressed as $V_0 = \text{Ma}_0 a_0$, with a_0 being the speed of sound at the given altitude H_0 . During the majority of the mission, particularly the midcourse phase, the vehicle operates at high speeds, suggesting high values of V_0 . This yields the following approximations:

$$mV_0 \gg \left| \frac{\partial f_\gamma}{\partial \vec{x}_0}(\vec{x}_0, \vec{u}_0) \delta\vec{x} + \frac{\partial f_\gamma}{\partial \vec{u}_0}(\vec{x}_0, \vec{u}_0) \delta\vec{u} \right|,$$

$$mV_0 \gg \left| \frac{\partial f_\chi}{\partial \vec{x}_0}(\vec{x}_0, \vec{u}_0) \delta\vec{x} + \frac{\partial f_\chi}{\partial \vec{u}_0}(\vec{x}_0, \vec{u}_0) \delta\vec{u} \right|.$$

These relationships suggest that, for the considered flight phase, the coupling between translational and rotational dynamics via the terms $\dot{\gamma}$ and $\dot{\chi}$ can be neglected. This leads to the following simplified and affine version of Eq. (3) around any equilibrium point $\vec{\rho}$:

$$\delta\vec{x}_1 = \begin{bmatrix} \delta\dot{\mu} \\ \delta\dot{\alpha} \\ \delta\dot{\beta} \end{bmatrix} = T_1(\vec{\rho}) \begin{bmatrix} \delta p \\ \delta q \\ \delta r \end{bmatrix}, \quad (23)$$

where $T_1(\vec{\rho})$ is a transformation matrix with dependencies on α and β (cf. Eq. (3)). In many applications, the contribution of the cross product in Eq. (2) can be assumed to be much smaller than the influence of the aerodynamic moments [32]. This allows in the first to simplify Eq. (2) as:

$$\delta\vec{x}_2 = \begin{bmatrix} \delta\dot{p} \\ \delta\dot{q} \\ \delta\dot{r} \end{bmatrix} = \mathbf{I}^{-1} \begin{bmatrix} \delta L \\ \delta M \\ \delta N \end{bmatrix}. \quad (24)$$

As discussed in Sect. II, only the aerodynamic, gravitational, centrifugal, and Coriolis forces and moments are initially regarded as relevant during the reentry phase since hypersonic glide vehicles are commonly unpowered during these mission stages. In a previous step, it was suggested that forces, and consequently also moments, induced by gravitation can be neglected for the control problem considered here. The same applies to forces and moments arising from centrifugal and Coriolis effects acting on the vehicle. Since these contributions have only a limited effect on the regarded dynamics, it is often well justified to neglect them when considering the attitude control of a flight vehicle [33]. With these simplifications, only aerodynamic moments remain, which can be modeled as functions of the scheduling parameter vector $\vec{\rho}$:

$$\begin{bmatrix} \delta L(\vec{\rho}) \\ \delta M(\vec{\rho}) \\ \delta N(\vec{\rho}) \end{bmatrix} = \underbrace{\bar{q} S l}_{\Gamma} \begin{bmatrix} \delta C_l(\vec{\rho}) \\ \delta C_m(\vec{\rho}) \\ \delta C_n(\vec{\rho}) \end{bmatrix}, \quad (25)$$

with \bar{q} being the dynamic pressure, S the aerodynamic reference area, and l the aerodynamic reference length (same for all axes here). The aerodynamic moment coefficients are usually nonlinear functions of the flow conditions, which in our case depends on the current flight parameters $\vec{\rho}$ and the states \vec{x} . To obtain a quasi-LPV representation, a Jacobian linearization approach was used in which the needed moment coefficient derivatives concerning the states $(\mu, \alpha, \beta, p, q, r)$ are modeled as functions of the scheduling parameters $\vec{\rho}$. That is, the nonlinear moment coefficients $(C_l(\vec{\rho}), C_m(\vec{\rho}), C_n(\vec{\rho}))$ are approximated as affine functions of the state vector $(\delta\mu, \delta\alpha, \delta\beta, \delta p, \delta q, \delta r)^T$:

$$\begin{bmatrix} \delta C_l(\vec{\rho}) \\ \delta C_m(\vec{\rho}) \\ \delta C_n(\vec{\rho}) \end{bmatrix} = \begin{bmatrix} C_{l,\mu}(\vec{\rho}) & C_{l,\alpha}(\vec{\rho}) & C_{l,\beta}(\vec{\rho}) & C_{l,p}(\vec{\rho}) & C_{l,q}(\vec{\rho}) & C_{l,r}(\vec{\rho}) \\ C_{m,\mu}(\vec{\rho}) & C_{m,\alpha}(\vec{\rho}) & C_{m,\beta}(\vec{\rho}) & C_{m,p}(\vec{\rho}) & C_{m,q}(\vec{\rho}) & C_{m,r}(\vec{\rho}) \\ C_{n,\mu}(\vec{\rho}) & C_{n,\alpha}(\vec{\rho}) & C_{n,\beta}(\vec{\rho}) & C_{n,p}(\vec{\rho}) & C_{n,q}(\vec{\rho}) & C_{n,r}(\vec{\rho}) \end{bmatrix} \begin{bmatrix} \delta\mu \\ \delta\alpha \\ \delta\beta \\ \delta p \\ \delta q \\ \delta r \end{bmatrix}. \quad (26)$$

The linearization procedure is performed across the four-dimensional space of the scheduling variables $\vec{\rho} = [\alpha \ \beta \ Ma \ H]^T$, delivering a multidimensional grid of aerodynamic coefficients needed to model the dynamics of the system. Fig. 6 illustrates the nonlinear dependencies for two of the most important derivatives, $C_{m,\alpha}(\vec{\rho})$ and $C_{l,\beta}(\vec{\rho})$, out of the 18 involved in Eq. (26). As the four-dimensional tables cannot be visualized, only two-dimensional slices are represented as three-dimensional surface plots: for $C_{m,\alpha}(\vec{\rho})$ the (Ma, α) slice corresponding to $H = 5000$ m and $\beta = 0^\circ$ is shown in Fig. 6a. The slice of $C_{l,\beta}(\vec{\rho})$ for $H = 5000$ m and $\alpha = 0^\circ$ is shown in Fig. 6b. The partial and incomplete view provided by these slices already shows that the model exhibits significant nonlinearities.

As explained earlier in Eqs. (8-9) and Fig. 4, the vehicle is over-actuated and a control allocation is used. The control input vector $\delta\vec{u}$ is defined as the perturbation virtual control command vector $\delta\vec{v} = (\delta\dot{p}, \delta\dot{q}, \delta\dot{r})^T$ and these inputs can directly be injected into the equations of \dot{p} , \dot{q} , and \dot{r} .

Eventually, the following quasi-LPV representation is obtained:

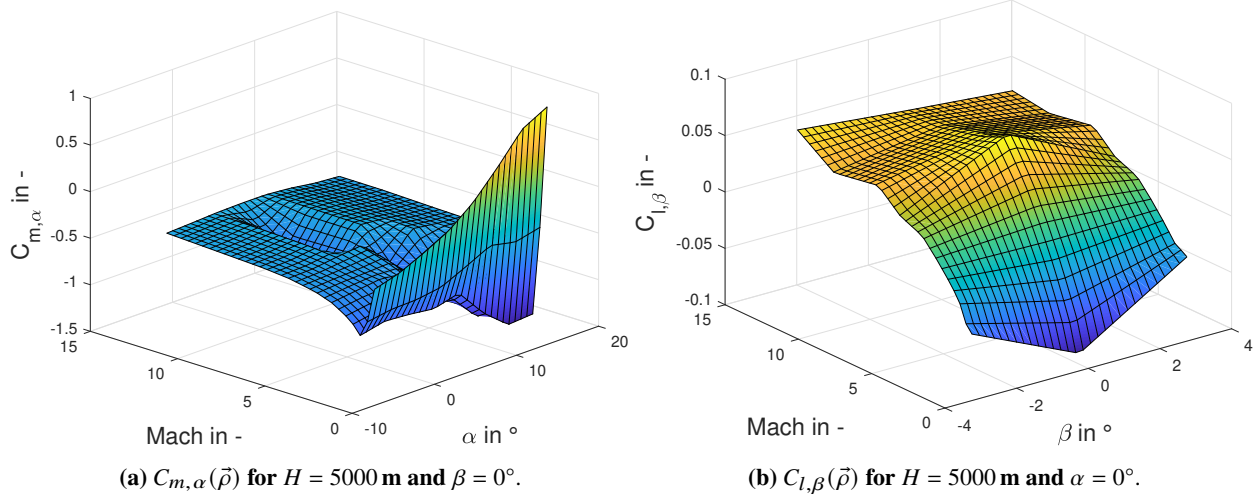


Figure 6 Examples of as state affine modeled aerodynamic moments across the generated grid data set.

$$\delta \dot{\vec{x}} = A(\vec{\rho}) \underbrace{\begin{bmatrix} \delta \mu \\ \delta \alpha \\ \delta \beta \\ \delta p \\ \delta q \\ \delta r \end{bmatrix}}_{\delta \vec{x}} + B(\vec{\rho}) \underbrace{\begin{bmatrix} \delta \dot{p} \\ \delta \dot{q} \\ \delta \dot{r} \end{bmatrix}}_{\delta \vec{u}}, \quad (27)$$

where

$$A(\vec{\rho}) = \begin{bmatrix} 0_{3 \times 3} & T_1(\vec{\rho}) \\ & \Xi(\vec{\rho}) \end{bmatrix}, \quad (28)$$

$$\text{with } \Xi(\vec{\rho}) = \mathbf{I}^{-1} \Gamma \begin{bmatrix} C_{l,\mu}(\vec{\rho}) & C_{l,\alpha}(\vec{\rho}) & C_{l,\beta}(\vec{\rho}) & C_{l,p}(\vec{\rho}) & C_{l,q}(\vec{\rho}) & C_{l,r}(\vec{\rho}) \\ C_{m,\mu}(\vec{\rho}) & C_{m,\alpha}(\vec{\rho}) & C_{m,\beta}(\vec{\rho}) & C_{m,p}(\vec{\rho}) & C_{m,q}(\vec{\rho}) & C_{m,r}(\vec{\rho}) \\ C_{n,\mu}(\vec{\rho}) & C_{n,\alpha}(\vec{\rho}) & C_{n,\beta}(\vec{\rho}) & C_{n,p}(\vec{\rho}) & C_{n,q}(\vec{\rho}) & C_{n,r}(\vec{\rho}) \end{bmatrix} \quad (29)$$

and with the following control effectiveness matrix $B(\vec{\rho})$:

$$B(\vec{\rho}) = \begin{bmatrix} 0_{3 \times 3} \\ I_{3 \times 3} \end{bmatrix}. \quad (30)$$

The defined control effectiveness matrix $B(\vec{\rho})$ allows designing the controller without directly having to consider the control surface effectiveness. The controller virtual commands v are transformed into moment commands using Eq. (7) and solved through the control allocation problem in Eq. (8). This representation does not consider actuator dynamics. In practice, if desired and when the actuators are able to follow the commands (i.e., not fully position- or rate-saturated), generic actuator dynamics could be modeled on the virtual commands by using low-pass filters with the appropriate bandwidth. This work focuses on the control architecture and the use of simplified models in an NDI-inspired approach, and for simplicity, the actuator dynamics are neglected (i.e., assumed to be sufficiently fast).

Remark 3 *It should be noted that the simplifications used for deriving the quasi-LPV dynamic model, particularly the neglect of gravitational effects, result in a justifiable but unavoidable deviation between the derived quasi-LPV model and the real nonlinear dynamics of the system. For instance, the gravitational force induces a constant downward*

acceleration that affects the time derivatives of the angle of attack and sideslip angle, depending on the flight path bank angle. Additionally, despite the fact that the cross-coupling terms in Eq. (2) have little influence on the fast dynamics and pointwise attitude changes, their neglect could lead to noticeable deviations in cases involving complex maneuvers with non-trivial rotational dynamics (i.e., significant variations in p , q , and r). In the current state of this work, these influences are neglected and not further discussed. However, in future work, such effects will be addressed as disturbances on the dynamics to enhance the accuracy of the derived quasi-LPV model and provide better robustness guarantees for controllers that are using the model for the control synthesis.

C. Comparison with LTI Models

During the derivation of the grid-based quasi-LPV model, several simplifications were made to transform the nonlinear dynamic behavior of HGVs during the midcourse into a quasi-LPV representation in Eq. (27). A comparison between local LTI models obtained by directly linearizing the full nonlinear model and simplified LPV model is performed to check the differences in behavior between both models. In the study, the poles obtained on the derived quasi-LPV model are compared to those of a local LTI model at the same flight conditions. The respective pole migration with changing Mach number and altitude are shown in Fig. 7a and Fig. 7b. The pole locations from the LTI model derived from the full nonlinear model are depicted using blue markers, while those from the simplified LPV model are represented with red markers.

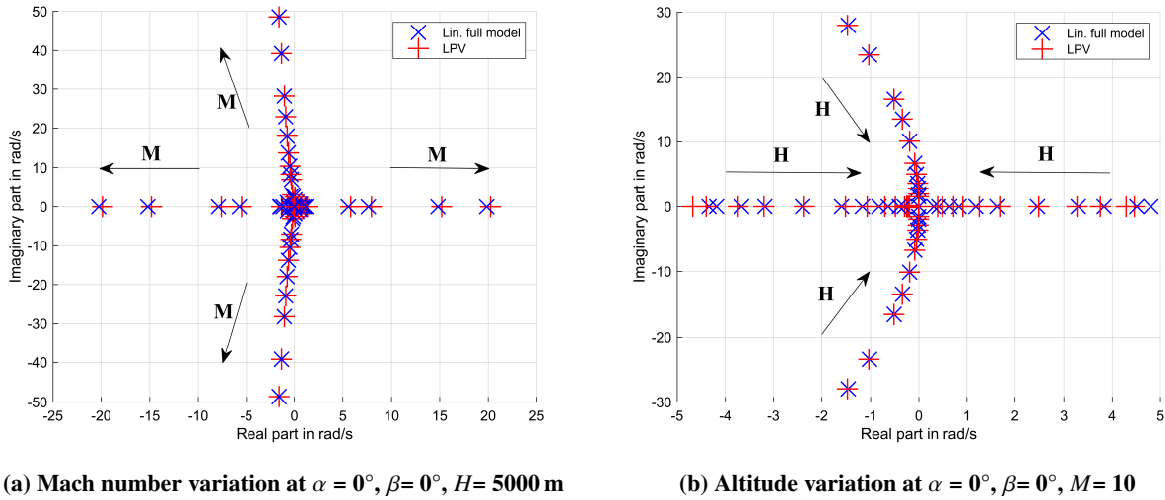


Figure 7 Pole-zero maps.

The presented analysis focuses on scenarios with variable altitudes and Mach numbers, maintaining zero angles of attack (α) and sideslip (β). Fig. 7a shows the pole migration over Mach number variations ($M=[5,20]$) at an altitude of 5 km. For the results shown in Fig. 7b the Mach number was maintained at 10 to investigate the differences in the pole location over variations in altitude. The good agreement between both models validates that only limited errors are introduced through the simplifications made.

V. Gain Determination Using Eigenstructure Assignment

The state-space realization of the quasi-LPV approximation at a parametrized operating point $\vec{\rho}$ derived above, cf. Eq (27), closely resembles the form of a generalized second-order system:

$$M\ddot{\vec{\varphi}} + D(\vec{\rho})\dot{\vec{\varphi}} + K(\vec{\rho})\vec{\varphi} = F\vec{u}_\varphi, \quad (31)$$

where $\vec{\varphi}$ is the generalized position vector $(\mu, \alpha, \beta)^T$, $\dot{\vec{\varphi}}$ the generalized velocity vector $(\dot{\mu}, \dot{\alpha}, \dot{\beta})^T$, M the mass matrix, $D(\vec{\rho})$ the damping matrix, $K(\vec{\rho})$ the stiffness matrix, $F = [0_{3 \times 3}, I_{3 \times 3}]^T$ the control effectiveness matrix and \vec{u}_φ the input vector $(\ddot{\mu}, \ddot{\alpha}, \ddot{\beta})^T$ [34]. Due to the generalized nature of the considered second-order dynamics, they can be further abstracted to directly address the dynamical properties. By applying the following relationship, which is further

discussed in [35], the differential equation can be rewritten in terms of the damping ratios $\zeta_i(\vec{\rho})$ and natural frequencies $\omega_i(\vec{\rho})$ with decoupled eigenmodes:

$$\vec{\varphi} + \underbrace{\begin{bmatrix} 2\zeta_\mu(\vec{\rho})\omega_\mu(\vec{\rho}) & 0 & 0 \\ 0 & 2\zeta_\alpha(\vec{\rho})\omega_\alpha(\vec{\rho}) & 0 \\ 0 & 0 & 2\zeta_\beta(\vec{\rho})\omega_\beta(\vec{\rho}) \end{bmatrix}}_{D(\vec{\rho})} \vec{\varphi} + \underbrace{\begin{bmatrix} \omega_\mu^2(\vec{\rho}) & 0 & 0 \\ 0 & \omega_\alpha^2(\vec{\rho}) & 0 \\ 0 & 0 & \omega_\beta^2(\vec{\rho}) \end{bmatrix}}_{K(\vec{\rho})} \vec{\varphi} = F\vec{u}_\varphi. \quad (32)$$

This equation is further reformulated to describe the regarded dynamics in a form similar to the previously derived state-space system, cf. Sect. IV, leading to:

$$\dot{\vec{x}}_\varphi = \begin{bmatrix} \dot{\vec{\varphi}} \\ \vec{\varphi} \end{bmatrix} = \underbrace{\begin{bmatrix} 0_{3 \times 3} & I_{3 \times 3} \\ -diag(\omega_i^2(\vec{\rho})) & -diag(2\zeta_i(\vec{\rho})\omega_i(\vec{\rho})) \end{bmatrix}}_{A_\varphi(\vec{\rho})} \underbrace{\begin{bmatrix} \vec{\varphi} \\ \vec{\varphi} \end{bmatrix}}_{\vec{x}_\varphi} + \underbrace{\begin{bmatrix} 0_{3 \times 3} \\ I_{3 \times 3} \end{bmatrix}}_{B_\varphi(\vec{\rho})} \vec{u}_\varphi. \quad (33)$$

Even though the derived relationship allows to define the damping and natural frequencies for a second-order system, the current state-space realization does not match the presented state-space form of Eq. (27), since $(\dot{\mu}, \dot{\alpha}, \dot{\beta})$ does not equal (p, q, r) . Hence, a similarity transformation is applied to change the state vector definition of the last derived state-space system from Eq.(33):

$$\vec{x}_\varphi = \tilde{T}(\vec{\rho})\delta\vec{x}, \quad (34)$$

where $\delta\vec{x}$ is the desired state vector $(\delta\mu, \delta\alpha, \delta\beta, \delta p, \delta q, \delta r)^T$ from Eq. (27) and $\tilde{T}(\vec{\rho})$ a linear transformation matrix, defined by:

$$\tilde{T}(\vec{\rho}) = \begin{bmatrix} I_{3 \times 3} & 0_{3 \times 3} \\ 0_{3 \times 3} & T_1(\vec{\rho}) \end{bmatrix}.$$

Applying the given similarity transformation on Eq. (33) via Eq. (34), we obtain:

$$\tilde{T}(\vec{\rho})\delta\dot{\vec{x}} = A_\varphi(\vec{\rho})\tilde{T}(\vec{\rho})\delta\vec{x} + B_\varphi(\vec{\rho})\vec{u}_\varphi. \quad (35)$$

Rearranging Eq. (35) yields:

$$\delta\dot{\vec{x}} = \underbrace{\tilde{T}^{-1}(\vec{\rho})A_\varphi(\vec{\rho})\tilde{T}(\vec{\rho})}_{\tilde{A}(\vec{\rho})} \delta\vec{x} + \underbrace{\tilde{T}^{-1}(\vec{\rho})B_\varphi(\vec{\rho})}_{\tilde{B}_\varphi(\vec{\rho})} \vec{u}_\varphi, \quad (36)$$

where

$$\tilde{A}(\vec{\rho}) = \begin{bmatrix} 0_{3 \times 3} & T_1(\vec{\rho}) \\ -T_1^{-1}(\vec{\rho})diag(2\zeta_i(\vec{\rho})\omega_i(\vec{\rho})) & -T_1^{-1}(\vec{\rho})diag(\omega_i^2(\vec{\rho}))T_1(\vec{\rho}) \end{bmatrix}$$

$$\tilde{B}_\varphi(\vec{\rho}) = \begin{bmatrix} 0_{3 \times 3} \\ T_1^{-1}(\vec{\rho}) \end{bmatrix}.$$

However, there is still a mismatch of the control input between the here derived generalized replacement model, which uses \vec{u}_φ , and the state space system in Eq. (27), which uses $\delta\vec{u}$. The input is transformed utilizing a method given in [19, 36]: by differentiating Eq(3) with respect to time, the following relationship between the body rotational accelerations and the angular accelerations is obtained:

$$\begin{bmatrix} \ddot{\mu} \\ \ddot{\alpha} \\ \ddot{\beta} \end{bmatrix} = T_1(\vec{\rho}) \begin{bmatrix} \dot{p} \\ \dot{q} \\ \dot{r} \end{bmatrix} + \dot{T}_1(\vec{\rho}) \begin{bmatrix} p \\ q \\ r \end{bmatrix} + T_2(\vec{\rho}) \begin{bmatrix} \dot{\gamma} \\ \dot{\chi} \end{bmatrix} + \dot{T}_2(\vec{\rho}) \begin{bmatrix} \dot{\gamma} \\ \dot{\chi} \end{bmatrix}. \quad (37)$$

Neglecting the translation-related terms containing $\dot{\gamma}$, $\dot{\chi}$, $\dot{\gamma}$, and $\dot{\chi}$, and assuming a time-scale separation between the considered dynamics and the matrix function \tilde{T}_1 ($\tilde{T}_1 \approx 0_{3 \times 3}$ is only violated under very aggressive maneuvers) the following simplification holds:

$$\vec{u}_\varphi = \begin{bmatrix} \ddot{\mu} \\ \ddot{\alpha} \\ \ddot{\beta} \end{bmatrix} = T_1(\vec{\rho})\vec{u} = T_1(\vec{\rho}) \begin{bmatrix} \dot{p} \\ \dot{q} \\ \dot{r} \end{bmatrix}. \quad (38)$$

This allows to formulate the following new control effectiveness matrix \tilde{B} for the considered replacement model:

$$\tilde{B}(\vec{\rho}) = \begin{bmatrix} 0_{3 \times 3} \\ I_{3 \times 3} \end{bmatrix}, \quad (39)$$

leading to:

$$\delta \dot{\vec{x}} = \tilde{A}(\vec{\rho})\delta \vec{x} + \tilde{B}(\vec{\rho})\delta \vec{u}. \quad (40)$$

The obtained state-space form allows solving the Eigenstructure assignment problem analytically by exploiting the generalized second-order structure of the system. The analytical expressions for the feedback gains of the cascaded nonlinear control are based on the terms previously derived for the quasi-LPV model from Eq. (27). Note, that the possibility of defining the desired closed-loop dynamics as a function of the scheduling parameters $\vec{\rho}$ remains, but the notation “ $(\vec{\rho})$ ” is dropped from now on, as it would be applied to most variables, affecting readability. The system is controlled by means of a static full-state feedback matrix K , such that the control input vector $\delta \vec{u}$ can be defined as:

$$\delta \vec{u} = -K\delta \vec{x}. \quad (41)$$

Applying the previously derived quasi-LPV model from Eq. (27) yields:

$$\delta \vec{x} = A\delta \vec{x} + B\delta \vec{u} = A\delta \vec{x} - BK\delta \vec{x} = \underbrace{(A - BK)}_{\tilde{A}} \delta \vec{x}, \quad (42)$$

where \tilde{A} is the desired closed-loop system matrix and is defined by setting the system matrix from Eq. (40) with desired pole locations (ω_i and ζ_i) and decoupled eigenmodes. By setting \tilde{A} in this way, not only the poles are being placed, but also the eigenvectors. Hence the following Eigenstructure assignment problem is solved for the considered generalized second-order system:

$$\tilde{A} = V\Lambda V^{-1}, \quad (43)$$

with

$$V = \begin{bmatrix} \xi_1 & \dots & \xi_n \end{bmatrix},$$

and

$$\Lambda = \begin{bmatrix} \lambda_1 & \dots & 0 \\ \vdots & \ddots & \vdots \\ 0 & \dots & \lambda_n \end{bmatrix},$$

where ξ_i are the n eigenvectors and $\lambda_i = a_i \pm b_i$ the corresponding eigenvalues [37]. The feedback gain matrix K follows as:

$$K = (B^T B)^{-1} B^T (A - \tilde{A}). \quad (44)$$

This approach allows computing the feedback control gain matrix K by considering both the current system dynamics, cf. Eq. (27), and the desired system dynamics, cf. Eq. (40). Hence, the presented method allows to place the closed-loop dynamics directly through the the desired system matrix \tilde{A} . The resulting feedback control gain matrix K takes the form of an $n \times m$ matrix, typically structured as:

$$K^T = \begin{bmatrix} K_1 & K_2 & K_3 & K_4 & K_5 & K_6 \\ K_7 & K_8 & K_9 & K_{10} & K_{11} & K_{12} \\ K_{13} & K_{14} & K_{15} & K_{16} & K_{17} & K_{18} \end{bmatrix}. \quad (45)$$

In theory, the proposed controller method can be used as an online solution, with real-time calculation of the gains using modern embedded systems. In this work, we opt for offline gain computation over the entire flight envelope. A gain scheduling approach is implemented, and the preferred gains are stored in lookup tables for the entire flight envelope. These gains can be directly utilized for full-state feedback, providing an approximately equivalent control approach

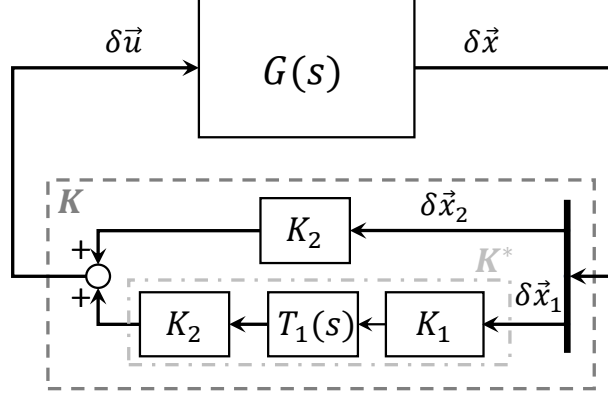


Figure 8 Illustration of abstracted cascaded inversion-based nonlinear flight control architecture.

to an NDI controller. Alternatively, the gains can be extracted for the cascaded NDI feedback control system. Fig. 8 illustrates how the feedback control matrix K is re-interpreted into a cascaded inversion-based nonlinear flight control architecture, where $G(s)$ is the abstracted plant that includes the open-loop systems dynamics from Eq.(27). By using the same assumptions as presented for the quasi-LPV model in Sect. IV for the derivation of Eq.(27), the gain matrix K is partitioned into the matrix elements K_2 and K^* :

$$K = \begin{bmatrix} K^* \\ K_2 \end{bmatrix} = \begin{bmatrix} K_1 & K_7 & K_{13} \\ K_2 & K_8 & K_{14} \\ K_3 & K_9 & K_{15} \\ K_4 & K_{10} & K_{16} \\ K_5 & K_{11} & K_{17} \\ K_6 & K_{12} & K_{18} \end{bmatrix}, \quad (46)$$

where K_2 is the inner-loop control gain matrix. As illustrated in Fig. 8, the other matrix element is given by:

$$K^* = K_2 T_1 K_1. \quad (47)$$

The gain matrix for the outer-loop controller is defined as:

$$K_1 = (K_2 T_1)^{-1} K^*. \quad (48)$$

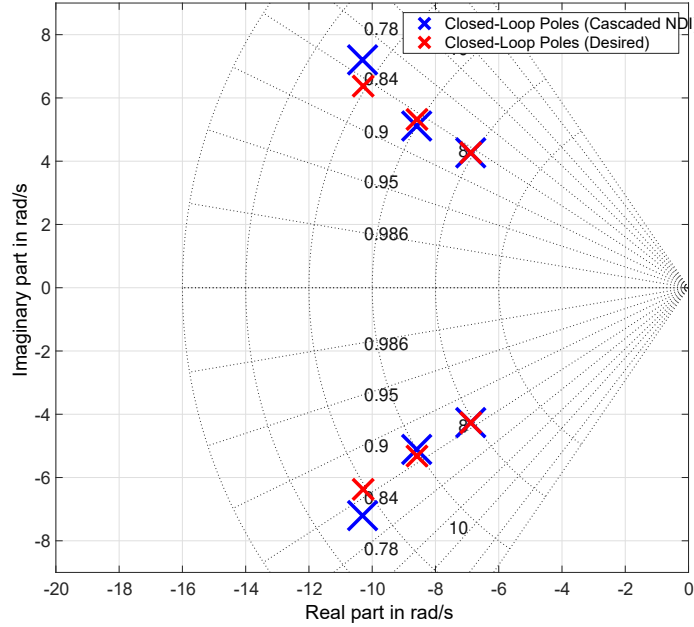
A. Comparison analysis of closed-loop system with cascaded NDI and desired Poles

In the following investigation, the effectiveness of the proposed Eigenstructure assignment method is evaluated by comparing the poles of the linearized closed-loop system with a cascaded nonlinear controller to the desired poles for a single operating point. The operating point is defined by $\alpha = 0^\circ$, $\beta = 0^\circ$, $H = 40\text{km}$, and $\text{Ma} = 12.5$. The desired pole locations are given in Table 1, and the closed-loop poles resulting from the proposed method are given in Fig. 9 and numerically in Table 1.

The obtained pole locations closely approximate their desired values, indicating that the proposed quasi-LPV approximation, in combination with Eigenstructure assignment, offers a valid method for determining the gain parameters of the cascaded nonlinear controller structure. While the analysis focuses on a single operating point, it is essential to note that similar results were obtained across various operating conditions. This suggests that desired pole locations can be met by the presented approach, even in sub-hypersonic flight regimes.

Table 1 Desired and obtained closed-loop poles of nonlinear cascaded controller.

Flight dynamics mode	Desired pole pair	Obtained pole pair
Bank angle related poles (μ, p)	$-6.8850 \pm 4.2669i$	$-6.8851 \pm 4.2637i$
Angle of attack related poles (α, q)	$-10.2850 \pm 6.3741i$	$-10.3048 \pm 7.2033i$
Sideslip angle related poles (β, r)	$-8.5850 \pm 5.3205i$	$-8.5935 \pm 5.1123i$

**Figure 9** Poles-zeros map: Comparison between the closed-loop system with the cascaded NDI applied to the nonlinear model and the desired pole locations.

VI. Simulation Results

A nonlinear simulation examined the control performance of the cascaded nonlinear control architecture, as presented in Sect. III, that uses gains determined via the proposed methodology. In the subsequent exemplary evaluation, the closed-loop control system is evaluated for the control performance of the nominal closed-loop system w.r.t pitch, roll and yaw maneuvers. The flight vehicle is trimmed and initiated at an altitude of 45 km and a Mach number of 12.5.

Fig. 10 presents the closed-loop system response to a sinusoidal input of increasing amplitude on the commanded angle of attack α_r . The reference command is in dash-dotted black, and the vehicle's response is displayed as a solid gray line.

The controller tracks the given reference signal on the angle of attack channel tightly. However, the closed-loop tracks with a small time delay due to the defined frequency of the desired closed-loop response. The actuator position limits are displayed in dashed red lines and are set to 20° for the upper limit and to 0° for the lower limit for each flap. The control allocation described in Sect. III distributes the commands on the four control surfaces, as expected. Upon reaching the position limits on the third and fourth actuators (a direct consequence of the increasing amplitude of the test signal), the algorithms start to use the first and second actuators for compensation. The integrated control allocation algorithm does not violate the defined limits and, as desired, no visible change in tracking behavior can be observed when this occurs. It needs to be noted that the differences in the magnitude between the upper and lower flap deflections can be explained due to the different flow conditions on the upper and lower side of the vehicle. This leads to a significantly higher control effectiveness for the lower flaps for cases in which the angle of attack of the vehicle are positive or zero. For cases with negative angle of attacks this effect turns around.

In the following lateral-directional maneuver case, α is held at 0° . The tracking performance in the roll channel

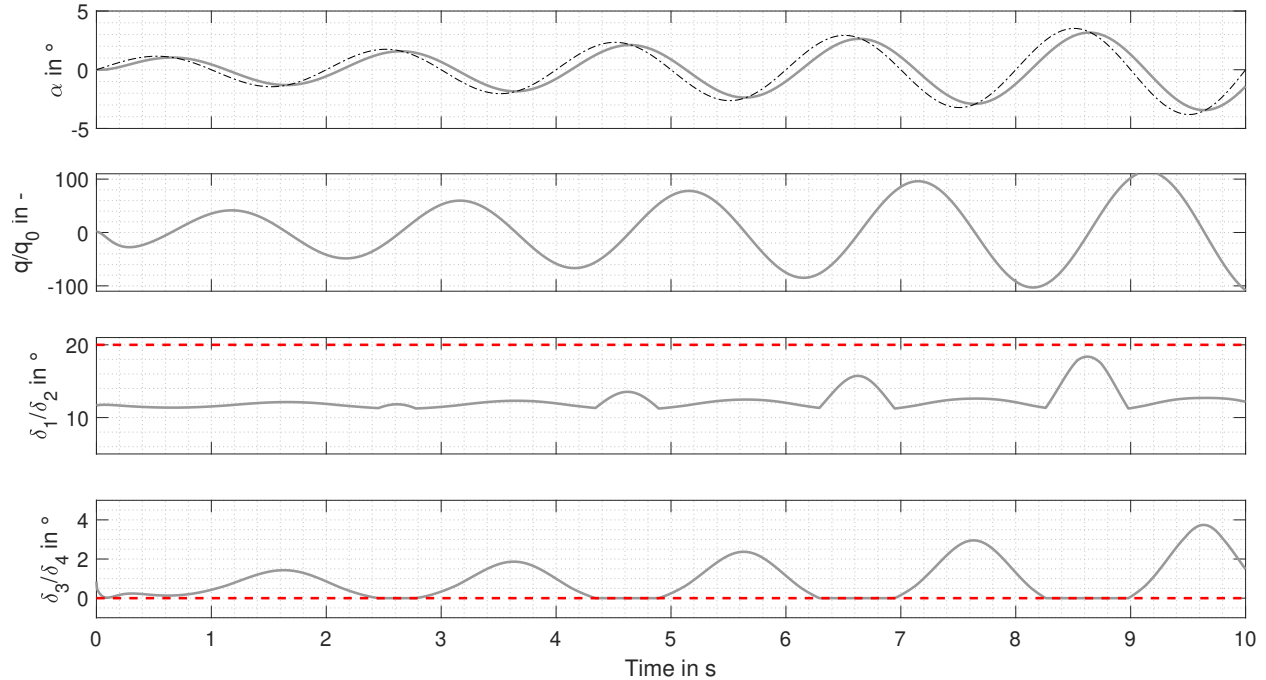


Figure 10 Simulation results for sinusoidal reference signal on the α channel. Displayed time series: angle of attack α , normalized pitch rate, and fin deflections in $^\circ$. Dash-dotted black: reference command, solid grey: vehicle response, dashed red: actuator deflection limits.

is evaluated by providing a doublet reference command on the μ_r channel with a magnitude of 5° at the beginning of the simulation. Later, the sideslip angle channel is tested also using a doublet command on the β_r channel with a magnitude of 1° . The time series show that the controller is able to follow both commands properly. Even though the sideslip reference command is smaller in magnitude, the control surface deflections are much more significant. This is because the system is not designed for operation at large slip angles, and the yaw effectiveness of the control surfaces is somewhat limited. The vehicle has good lateral static stability so that the directional stability quickly compensates the limited yaw moment of the control surface during the slip. The system also exhibits a strong yaw-roll coupling, which has to be compensated.

VII. Summary and Future Work

This paper introduces a gain-scheduling methodology for cascaded NDI-based controllers of HGVs. Grid-based quasi-LPV models are leveraged to facilitate the gain-scheduling by working directly with a representative yet simplified quasi-LPV model of the vehicle. While the approach can be used with a wide range of controller tuning techniques, it was demonstrated on a parameter-dependent analytical eigenstructure assignment example. The considered application and attitude control of a hypersonic glide vehicle yield a system dynamic approximated as a generalized second-order system. Due to the generalization of the open-loop system as a second-order structure, the Eigenstructure assignment problem is relatively easily solved analytically. The controller's application to the nonlinear simulation model shows a good agreement with the specifications used for the Eigenstructure assignment problem.

Future work will explore control methodologies capable of addressing bounded parametric uncertainties within the derived quasi-LPV dynamics, such as those related to aerodynamic coefficients, and additional bounded disturbances to account for modeling errors. The goal is to investigate robust control techniques that ensure reliable performance. Furthermore, the memory footprint of the implemented grid-based quasi-LPV controller could be improved based on a trade-off analysis between the grid-table size/resolution and the accuracy of the grid-based quasi-LPV model.

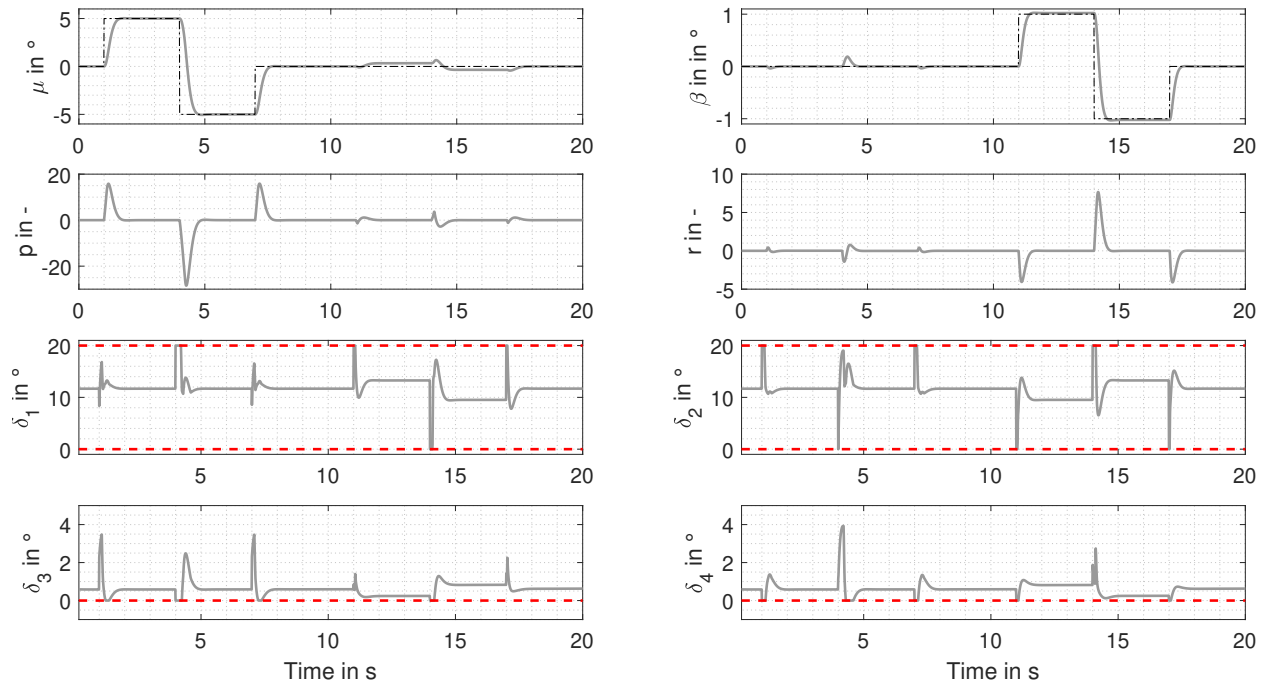


Figure 11 Simulation results for doublet signal on the μ and β channel. Displayed time series: aerodynamic bank angle μ , sideslip angle β , normalized pitch rate, and fin deflections in $^\circ$. Dash-dotted black: raw reference command, solid grey: vehicle response for NMFC without anti-windup system, dashed red: actuator deflection limits.

References

- [1] Slayer, K. M., "Hypersonic Weapons: Background and Issues for Congress," Tech. rep., Congressional Research Service, 2023. URL <https://crsreports.congress.gov/product/pdf/R/R45811/35>.
- [2] Göge, D., Zimper, D., Besser, H., Huggins, M., and Alan, S., "Hypersonic Vehicles - Game Changers for Future Warfare?" *Transforming Joint Air Power: The Journal of the JAPCC*, 2017.
- [3] Acquatella, P., Kampen, E.-J. V., and Chu, Q. P., "A Sampled-Data Form of Incremental Nonlinear Dynamic Inversion for Spacecraft Attitude Control," *AIAA SCITECH 2022 Forum*, 2022. <https://doi.org/10.2514/6.2022-0761>.
- [4] Holzapfel, F., "Nonlinear adaptive control of an unmanned aerial vehicle (Original German Title: Nichtlineare adaptive Regelung eines unbemannten Fluggerätes)," Ph.D. thesis, Technische Universität München, München, Germany, Jun. 2004.
- [5] da Costa, R. R., Chu, Q. P., and Mulder, J. A., "Reentry Flight Controller Design Using Nonlinear Dynamic Inversion," *Journal of Spacecraft and Rockets*, Vol. 40, No. 1, 2003, pp. 64–71. <https://doi.org/10.2514/2.3916>.
- [6] Snell, S. A., Enns, F. D., and Garrard, W. L., "Nonlinear Inversion Flight Control for a Supermaneuverable Aircraft," *Journal of Guidance, Control, and Dynamics*, Vol. 15, No. 4, 1992, pp. 976–984. <https://doi.org/10.2514/3.20932>.
- [7] Menon, P., Iragavarapu, V., and Ohlmeyer, E., "Nonlinear missile autopilot design using time-scale separation," *AIAA Guidance, Navigation, and Control Conference*, 1997. <https://doi.org/10.2514/6.1997-3765>.
- [8] Lee, H., Reiman, S., Dillon, C., and Youssef, H., "Robust Nonlinear Dynamic Inversion Control for a Hypersonic Cruise Vehicle," *AIAA Guidance, Navigation and Control Conference and Exhibit*, 2007. <https://doi.org/10.2514/6.2007-6685>.
- [9] Reiner, J., Balas, G. J., and Garrard, W. L., "Flight control design using robust dynamic inversion and time-scale separation," *Automatica*, Vol. 32, No. 11, 1996, pp. 1493–1504. [https://doi.org/https://doi.org/10.1016/S0005-1098\(96\)00101-X](https://doi.org/https://doi.org/10.1016/S0005-1098(96)00101-X).
- [10] Wang, Q., and Stengel, R., "Robust nonlinear flight control of a high-performance aircraft," *IEEE Transactions on Control Systems Technology*, Vol. 13, No. 1, 2005, pp. 15–26. <https://doi.org/10.1109/TCST.2004.833651>.

- [11] Papageorgiou, C., and Glover, K., "Robustness Analysis of Nonlinear Flight Controllers," *Journal of Guidance, Control, and Dynamics*, Vol. 28, No. 4, 2005, pp. 639–648. <https://doi.org/10.2514/1.9389>.
- [12] Autenrieb, J., Fezans, N., Gruhn, P., and Klevanski, J., "Towards a Control-Centric Modelling and Simulation-Framework for Hypersonic Glide Vehicles," *German Aeronautics and Space Congress (DLRK)*, Bremen, Germany, 2021.
- [13] Gerhold, T., "Overview of the Hybrid RANS Code TAU," *MEGAFLOW - Numerical Flow Simulation for Aircraft Design*, edited by N. Kroll and J. K. Fassbender, Springer Berlin Heidelberg, Berlin, Heidelberg, 2005, pp. 81–92. https://doi.org/10.1007/3-540-32382-1_5.
- [14] Gerhold, T., "Overview of the Hybrid Rans Code TAU," *Notes on Numerical Fluid Mechanics and Multidisciplinary Design*, Vol. 89, 2002. https://doi.org/10.1007/3-540-32382-1_5.
- [15] "Flight dynamics – Concepts, quantities and symbols – Part 1: Aircraft motion relative to the air," Standard, International Organization for Standardization (ISO), Geneva, Switzerland, Apr. 1988. ISO 1151-1:1988.
- [16] "Flight dynamics – Concepts, quantities and symbols – Part 2: Motions of the aircraft and the atmosphere relative to the Earth," Standard, International Organization for Standardization (ISO), Geneva, Switzerland, Sep. 1985. ISO 1151-2:1985.
- [17] Young, T., *International Standard Atmosphere (ISA) Table*, Wiley, 2017, pp. 583–590. <https://doi.org/10.1002/9781118534786.app1>.
- [18] Ehernberger, L. J., "Stratospheric turbulence measurements and models for aerospace planedesign," *4th IAA Conference on Space Situational Awareness*, 1992. <https://doi.org/10.2514/6.1992-5072>.
- [19] Autenrieb, J., and Fezans, N., "Flight control design for a hypersonic waverider configuration: A non-linear model following control approach," *CEAS Space Journal*, 2024, pp. 1–24. <https://doi.org/10.1007/s12567-024-00544-0>.
- [20] Johansen, T., Fossen, T., and Berge, S., "Constrained nonlinear control allocation with singularity avoidance using sequential quadratic programming," *IEEE Transactions on Control Systems Technology*, Vol. 12, No. 1, 2004, pp. 211–216. <https://doi.org/10.1109/TCST.2003.821952>.
- [21] Härkegård, O., "Dynamic Control Allocation Using Constrained Quadratic Programming," *Journal of Guidance, Control, and Dynamics*, Vol. 27, No. 6, 2004, pp. 1028–1034. <https://doi.org/10.2514/1.11607>.
- [22] Autenrieb, J., and Gruhn, P., "An Iterative Dynamic Control Allocation Formulation for Hypersonic Vehicles with Asymmetrical Input Limitations on Magnitude and Rate," *AIAA SCITECH 2025 Forum*, 2025.
- [23] Stevens, B., Lewis, F., and Johnson, E., *Aircraft Control and Simulation: Dynamics, Controls Design, and Autonomous Systems, Third Edition*, John Wiley & Sons, 2015. <https://doi.org/10.1002/9781119174882>.
- [24] Slotine, J.-J. E., and Li, W., *Applied nonlinear control*, Prentice Hall, 1991.
- [25] Shamma, J. S., and Cloutier, J. R., "Gain-scheduled missile autopilot design using linear parameter varying transformations," *Journal of Guidance, Control, and Dynamics*, Vol. 16, No. 2, 1993, pp. 256–263. <https://doi.org/10.2514/3.20997>.
- [26] Leith, D. J., and Leithead, W. E., "Survey of gain-scheduling analysis and design," *International Journal of Control*, Vol. 73, No. 11, 2000, pp. 1001–1025. <https://doi.org/10.1080/002071700411304>.
- [27] Sève, F., Theodoulis, S., Wernert, P., Zasadzinski, M., and Boutayeb, M., "Flight Dynamics Modeling of Dual-Spin Guided Projectiles," *IEEE Transactions on Aerospace and Electronic Systems*, Vol. 53, No. 4, 2017, pp. 1625–1641. <https://doi.org/10.1109/TAES.2017.2667820>.
- [28] Marcos, A., and Balas, G., "Development of Linear-Parameter-Varying Models for Aircraft," *Journal of Guidance Control Dynamics*, Vol. 27, 2004, pp. 218–228. <https://doi.org/10.2514/1.9165>.
- [29] Vinco, G., Theodoulis, S., Sename, O., and Strub, G., "Quasi-LPV Modeling of Guided Projectile Pitch Dynamics through State Transformation Technique," *IFAC-PapersOnLine*, Vol. 55, No. 35, 2022, pp. 43–48. <https://doi.org/https://doi.org/10.1016/j.ifacol.2022.11.288>.
- [30] Pfifer, H., "LPV/LFT Modeling and its Application in Aerospace," Ph.D. thesis, Technische Universität München, München, Germany, Feb. 2013.
- [31] Lee, C. H., and Chung, M. J., "Gain-scheduled state feedback control design technique for flight vehicles," *IEEE Transactions on Aerospace and Electronic Systems*, Vol. 37, No. 1, 2001, pp. 173–182. <https://doi.org/10.1109/7.913676>.

- [32] Tekin, R., and Pfifer, H., "Linear Parameter Varying Control of an Agile Missile Model Based on the Induced L2-norm Framework," *CEAS EuroGNC "Conference on Guidance, Navigation and Control"*, 2013, pp. 3–14. https://doi.org/10.1007/978-3-642-38253-6_1.
- [33] Pfifer, H., "Quasi-LPV Model of a NDI-Controlled Missile Based on Function Substitution," *AIAA Guidance, Navigation, and Control Conference*, 2012. <https://doi.org/10.2514/6.2012-4970>.
- [34] Alazard, D., Fezans, N., and Imbert, N., "Mixed H2-Hinfinity control design for mechanical systems: analytical and numerical developments," 2008. <https://doi.org/10.2514/6.2008-7308>.
- [35] Fezans, N., Alazard, D., Imbert, N., and Carpentier, B., "Robust LPV control design for a RLV during reentry," *AIAA Guidance, Navigation, and Control Conference*, 2010. <https://doi.org/10.2514/6.2010-8194>.
- [36] Kiehn, D., "Stability Analysis and Flight Control Design of the Winged Reusable Launch Vehicle ReFEx," *CEAS Space Journal*, Vol. 13, 2021, pp. 51–64. <https://doi.org/10.1007/s12567-020-00319-3>.
- [37] Andry, A., Shapiro, E., and Chung, J., "Eigenstructure Assignment for Linear Systems," *IEEE Transactions on Aerospace and Electronic Systems*, Vol. AES-19, No. 5, 1983, pp. 711–729. <https://doi.org/10.1109/TAES.1983.309373>.